ACCRETION ONTO BLACK HOLES FROM LARGE SCALES REGULATED BY RADIATIVE FEEDBACK. II.
GROWTH RATE AND DUTY CYCLE

KwangHo Park and Massimo Ricotti

Department of Astronomy, University of Maryland, College Park, MD 20740, USA

kpark@astro.umd.edu, ricotti@astro.umd.edu

ABSTRACT

This paper, the second of a series on radiation-regulated accretion onto black holes (BHs) from galactic scales, focuses on the effects of radiation pressure and angular momentum of the accreting gas. We simulate accretion onto intermediate-mass black holes, but we derive general scaling relationships that are solutions of the Bondi problem with radiation feedback valid for any mass of the BH $M_{\rm bh}$. Thermal pressure of the ionized sphere around the BH regulates the accretion rate producing periodic and short-lived luminosity bursts. We find that for ambient gas densities exceeding $n_{\rm H,\infty}^{\rm cr} \propto M_{\rm bh}^{-1}$, the period of the oscillations decreases rapidly and the duty cycle increases from 6%, in agreement with observations of the fraction of active galactic nuclei at $z \sim 3$, to 50%. The mean accretion rate becomes Eddington limited for $n_{\rm H,\infty} > n_{\rm H,\infty}^{\rm Edd} \simeq n_{\rm H,\infty}^{\rm cr} T_{\infty,4}^{-1}$ where $T_{\infty,4}$ is the gas temperature in units of 10^4 K. In the sub-Eddington regime, the mean accretion rate onto BHs is about $1\% T_{\infty,4}^{2.5}$ of the Bondi rate, thus is proportional to the thermal pressure of the ambient medium. The period of the oscillations coincides with depletion timescale of the gas inside the ionized bubble surrounding the BH. Gas depletion is dominated by a pressure gradient pushing the gas outward if $n_{\rm H,\infty} < n_{\rm H,\infty}^{\rm cr}$ and by accretion onto the BH otherwise. Generally, for $n_{\rm H,\infty} < n_{\rm H,\infty}^{\rm cr}$ angular momentum does not affect significantly the accretion rate and period of the oscillations.

Subject headings: accretion, accretion disks – black hole physics – dark ages, reionization, first stars – hydrodynamics – methods: numerical – radiative transfer

1. INTRODUCTION

Gravitational accretion onto point sources can be described analytically (Bondi & Hoyle 1944; Bondi 1952) assuming spherical symmetry. The Eddington-limited Bondi formula is often prescribed in cosmological simulations to estimate the gas accretion rate onto black holes (BHs) from large scales (Volonteri & Rees 2005; Di Matteo, Colberg, Springel, Hernquist, & Sijacki 2008; Pelupessy, Di Matteo, & Ciardi 2007; Greif, Johnson, Klessen, & Bromm 2008; Alvarez, Wise, & Abel 2009; Kim, Wise, Alvarez, & Abel 2011). However, even in sub-Eddington regime, a fraction of the gravitational potential energy of accreted gas is

converted into mechanical or radiative feedback (Shapiro 1973), reducing the accretion rate. The radiation emitted by BHs creates feedback loops that regulate the gas accretion and luminosity of the BHs. Several published works have investigated physical processes that may dominate the feedback such as X-ray preheating, gas cooling, photo-heating, and radiation pressures (Ostriker, Weaver, Yahil, & McCray 1976; Cowie, Ostriker, & Stark 1978; Bisnovatyi-Kogan & Blinnikov 1980; Krolik & London 1983; Vitello 1984; Wandel, Yahil, & Milgrom 1984; Milosavljević, Bromm, Couch, & Oh 2009a; Ostriker, Choi, Ciotti, Novak, & Proga 2010; Novak, Ostriker, & Ciotti 2011). In general, radiative feedback reduces the accretion luminosity of the accreting BH (Ostriker, Weaver, Yahil, & McCray 1976; Begelman 1985; Ricotti, Ostriker, & Mack 2008). There have been extensive publications on self-regulation of supermassive BH growth at the centers of elliptical galaxies (Sazonov, Ostriker, Ciotti, & Sunyaev 2005; Ciotti & Ostriker 2007; Ciotti, Ostriker, & Proga 2009; Lusso & Ciotti 2011) or axisymmetric outflows in active galactic nuclei (AGNs; Proga 2007; Proga, Ostriker, & Kurosawa 2008; Kurosawa, Proga, & Nagamine 2009; Kurosawa & Proga 2009a,b). Recently, several works have paid closer attention to radiation-regulated accretion onto intermediate-mass black holes (IMBHs; Milosavljević, Bromm, Couch, & Oh 2009a; Milosavljević, Couch, & Bromm 2009b; Park & Ricotti 2011; Li 2011).

Cosmological simulations show that massive BHs may have formed in metal-free minihalos as Population III star remnants in the early universe (Abel, Anninos, Norman, & Zhang 1998; Bromm, Coppi, & Larson 1999; Abel, Bryan, & Norman 2000; Madau & Rees 2001; Schneider, Ferrara, Natarajan, & Omukai 2002; Oh & Haiman 2002) or from direct collapse of primordial gas (Carr, Bond, & Arnett 1984; Haehnelt, Natarajan, & Rees 1998; Fryer, Woosley, & Heger 2001; Begelman, Volonteri, & Rees 2006; Volonteri, Lodato, & Natarajan 2008; Omukai, Schneider, & Haiman 2008; Regan & Haehnelt 2009; Mayer, Kazantzidis, Escala, & Callegari 2010; Johnson, Khochfar, Greif, & Durier 2011). Estimating the accretion luminosity of IMBHs (for a review, see Miller & Colbert 2004; van der Marel 2004) is important to understand their cosmological importance at high z and in the local universe (Mack, Ostriker, & Ricotti 2007; Ricotti 2009). Since the luminosity of IMBHs is directly related to their accretion rate, these studies are also relevant for better understanding the mass growth of primordial massive BHs in the early universe (Madau & Rees 2001; Volonteri, Haardt, & Madau 2003; Yoo & Miralda-Escudé 2004; Volonteri & Rees 2005; Johnson & Bromm 2007; Pelupessy, Di Matteo, & Ciardi 2007; Alvarez, Wise, & Abel 2009) or provide clues about the origin and impact on the ionization history of the universe of ultraluminous X-ray sources (ULXs; Krolik, McKee, & Tarter 1981; Krolik & Kallman 1984; Krolik 2004; Ricotti & Ostriker 2004; Ricotti, Ostriker, & Gnedin 2005; Ricotti 2007; Strohmayer & Mushotzky 2009).

In Park & Ricotti (2011), hereafter Paper I, we explored the radiation-regulated accretion onto IMBHs assuming spherical symmetry and zero angular momentum of the accreting gas. One of the main objectives of the study was to derive an analytical description of the effect of radiation feedback on the Bondi accretion rate. We accomplished this goal by simulating accretion onto IMBHs with idealized initial conditions and simple physics, but for a large parameter space of the initial conditions (varying BH radiative efficiency, the BH mass, the density and temperature of ambient gas, and the spectrum of radiation). We found that the IMBH is quiescent most of the time with short intense periodic bursts of accretion (with duty cycle of 6%). The qualitative description of the cycle is as follows. Gas accumulates in a dense shell ahead of

the I-front nearly halting accretion onto the IMBH. Meanwhile, the ionized gas inside the hot bubble is pushed outward toward the dense shell by pressure gradients, eventually de-pressurizing the hot bubble, producing the collapse of the shell and a burst of accretion. The scaling relationships for the burst period, mean and peak accretion rates can be understood analytically but are quite sensitive to the details of the thermal structure inside the Strömgren sphere. Thus, we expect that gas metallicity may be an important parameter in the problem that we have not yet explored.

In this paper, the second of the series, we relax most of the simplifying assumptions in Paper I and discuss the effects of helium heating/cooling, radiation pressure, and gas angular momentum on the accretion rate. It has been noted that not only electron scattering but also radiation pressure on H I may be important (Milosavljević et al. 2009a). We explore how the radiation pressure regulates the gas accretion by transferring momentum to the inflowing gas, and whether these physical processes become important compared to the pressure gradients inside the Strömgren sphere.

As in Paper I of this series, here we present the results of our simulations as dimensionless accretion rates $\lambda_{\mathrm{rad}} \equiv \dot{M}/\dot{M}_B$, where $\dot{M}_B = \pi e^{3/2} \rho_\infty G^2 M_{\mathrm{bh}}^2 c_{s,\infty}^{-3}$ is the Bondi accretion rate for an isothermal gas (with polytropic index $\gamma = 1$), that is a function of BH mass M_{bh}, density ρ_∞, and sound speed of $c_{s,\infty}$ of neighboring gas. The Eddington luminosity is $L_{\mathrm{Edd}} = 4\pi G M_{\mathrm{bh}} m_p c \sigma_{\mathrm{T}}^{-1}$, which is proportional to the BH mass only. We define the Eddington accretion rate $\dot{M}_{\mathrm{Edd}} \equiv L_{\mathrm{Edd}}/c^2$ which is a factor of 10 smaller than the definition most often used $\dot{M}_{\mathrm{Edd}} \equiv L_{\mathrm{Edd}}/0.1c^2$, in which $\eta = 0.1$ is assumed, and the dimensionless Eddington rate as $\lambda_{\mathrm{Edd}} \equiv \eta^{-1} \dot{M}_{\mathrm{Edd}}/\dot{M}_B$. We introduced three quantities to describe the accretion: mean accretion rate $\langle \lambda_{\mathrm{rad}} \rangle$, accretion rate at peaks $\lambda_{\mathrm{rad,max}}$, and period between accretion bursts τ_{cycle}. In Paper I we found

$$\langle \lambda_{\mathrm{rad}} \rangle \simeq C(n_{\mathrm{H},\infty}) \, T_{\infty,4}^{2.5} \left[T_{\mathrm{in}}(\alpha, Z)/4 \times 10^4 \ \mathrm{K} \right]^{-4}, \tag{1}$$

with $C \sim 3\%$ for $n_{\mathrm{H},\infty} \geq 10^5 \ \mathrm{cm}^{-3}$ and $C \sim 3\%(n_{\mathrm{H},\infty}/10^5 \ \mathrm{cm}^{-3})^{1/2}$ for $n_{\mathrm{H},\infty} < 10^5 \ \mathrm{cm}^{-3}$ with $\eta = 0.1$ and $M_{\mathrm{bh}} = 100 \ M_\odot$. Here, $T_{\mathrm{in}}(\alpha, Z)$ is the time-averaged temperature at the accretion radius within the Strömgren sphere, that is $4 \times 10^4 \ \mathrm{K}$ for our fiducial spectrum (spectral slope $\alpha = 1.5$) and a gas composed of hydrogen only (metallicity $Z = 0$). However, T_{in} is sensitive to changes of α and the gas composition (see Paper I and Section 3 in this paper). In the sub-Eddington regime, the period $\tau_{\mathrm{cycle}} \propto \langle R_s \rangle$ where $\langle R_s \rangle$ is the time-averaged Strömgren radius, and the duty cycle $f_{\mathrm{duty}} \equiv \tau_{\mathrm{on}}/\tau_{\mathrm{cycle}} \equiv \langle \lambda_{\mathrm{rad}} \rangle/\lambda_{\mathrm{rad,max}} \sim 6\% \ T_{\infty,4}^{1/2}$, where τ_{on} is the duration of bursts.

This paper is organized as follows. In Section 2, we briefly explain the numerical methods. In Section 3, we present our simulation results including the effect of helium cooling/heating, radiation pressure, and gas angular momentum. Summary and discussion are presented in Section 4.

2. NUMERICAL SIMULATIONS

We run a suite of hydrodynamic simulations to interpret how radiative feedback regulates accretion onto BHs. We use a modified parallel non-relativistic hydrodynamics code, ZEUS-MP (Stone & Norman 1992; Hayes et al. 2006) plus a radiative transfer algorithm (Ricotti et al. 2001) to simulate photo-ionization

and photo-heating by UV and X-ray ionizing photons emitted near the BHs. See Paper I for a detailed description.

In this study, we include the effects of helium heating/cooing in addition to hydrogen. Therefore, we simulate photo-ionization, photo-heating and cooling for six species H I, H II, He I, He II, He III, and e^-.

We also calculate the radiation pressures both on e^- and H I to interpret the effect of momentum transfer to the inflowing gas by the ionizing photons. The magnitude of acceleration at a given radius due to radiation pressure depends on the luminosity, the ionization fraction of hydrogen and helium, and the cross section of the species to photon-ionization. The specific flux $F_\nu \propto e^{-\tau}/r^2$ at a given radius(r), assuming a power-law spectrum with a spectral index α, depends on the optical depth τ_ν, and the cross section σ_ν. Thus, the accelerations due to momentum transfer to H I and e^- can be written as

$$a_{\rm rad,H\ I} = \frac{x_{\rm H\ I}}{m_p c} \int \sigma_{\rm H\ I,\nu} F_\nu d\nu, \tag{2}$$

$$a_{\rm rad,e^-} = \frac{x_{e^-}}{m_p c} \int \sigma_T F_\nu d\nu, \tag{3}$$

where $x_{\rm H\ I}$ and x_{e^-} are H I and e^- fractions, respectively, σ_T is the Thomson cross section, and m_p is the proton mass. The radial component of the acceleration at a given radius is updated as $\mathbf{a} = \mathbf{a}_{\rm grav} + \mathbf{a}_{\rm rad}$, where $\mathbf{a}_{\rm rad} = \mathbf{a}_{\rm rad,H\ I} + \mathbf{a}_{\rm rad,e^-}$.

In Section 3.3, we study the effect of non-zero angular momentum of gas which leads to a time delay between the accretion rate at the sonic radius and the luminosity output, due to the formation of an accretion disk. In order to estimate realistic values of the time delay we assume that the gas conserves angular momentum and settles into an accretion disk of radius $R_{\rm disk}$. We then assume an alpha model for the thin disk to estimate the timescale for the gas to lose angular momentum and fall into the BH.

Numerically, it is convenient to express the time delay in units of the free-fall timescale $t_{\rm ff}$ calculated at the simulation's inner boundary (typically $R_{\rm min} \sim 10^{-5}$ pc). The free-fall timescale we have defined can be very large compared to $t_{\rm ff}$ calculated at the radius of the accretion disk near the BH (at tens of gravitational radii $R_{\rm Sch} \equiv 2GM_{\rm bh}/c^2$). Approximately, the gas is accreted at the viscous timescale $t_{\rm visc}$, that compared to $t_{\rm ff}$ is

$$t_{\rm visc}(R_{\rm disk})/t_{\rm ff}(R_{\rm disk}) \sim \alpha^{-1}\mathcal{M}^2 \sim \alpha^{-1} c_{\rm s,disk}^{-2} GM_{\rm bh} R_{\rm disk}^{-1} \sim 0.5\,\alpha^{-1}(c/c_{\rm s,disk})^2 \mathcal{R}_{\rm disk}^{-1}, \tag{4}$$

where α is the dimensionless parameter for a thin disk (Shakura & Sunyaev 1973), $c_{\rm s,disk}$ is the sound speed of the gas in the disk, and we define $\mathcal{R}_{\rm disk} \equiv R_{\rm disk}/R_{\rm Sch}$. The dependence of the free-fall time on radius is $t_{\rm ff} \propto R^{1.5}$, while the viscous timescales as $t_{\rm visc} \propto R^{-1}t_{\rm ff} \propto R^{0.5}$ assuming constant sound speed due to effective cooling (note that since we are considering a gas of zero or very low metallicity, the gas in the disk will not easily cool to temperature below 10^4 K if the gas is atomic). Thus, the infall time at the disk radius $R_{\rm disk}$ is

$$\frac{t_{\rm visc}(R_{\rm disk})}{t_{\rm ff}(R_{\rm min})} \sim \frac{0.5}{\alpha}\frac{v_{\rm min}^3}{c\,c_{\rm s,disk}^2}\mathcal{R}_{\rm disk}^{1/2} \sim \frac{0.3}{\alpha}\left(\frac{T_{\rm disk}}{10^4\ {\rm K}}\right)^{-1}\mathcal{R}_{\rm disk}^{1/2}. \tag{5}$$

To estimate the parameters in Equation (5) we have defined $v_{\min} \equiv (GM_{\rm bh}/R_{\min})^{1/2} \simeq 260$ km s^{-1}. Assuming $\alpha \sim 0.01$–0.1, $T_{\rm disk} \sim 10^4$ K, and $\mathcal{R}_{\rm disk} \lesssim 10^2$–$10^4$, we find time delays of $\lesssim 300$ free-fall times at $R_{\min}$, that is the parameter space we explore in Section 3.3.

In our code, the accretion rates calculated at the inner boundary of the simulations are stored in an assigned array about 1000 steps for each $t_{\rm ff}$. Stored accretion rates with a given time delay are then read from the array and used to estimate the luminosity at the current moment.

3. RESULTS

In this section, we show the results of simulations discussing the effects of helium heating/cooling, radiation pressures, and angular momentum on the BH accretion rate. All the simulations in this paper include helium heating/cooling but the gas is metal free. The simulations remain qualitatively the same as in Paper I where we did not include helium; the only noticeable difference with respect to Paper I is that the accretion rate at peak luminosity shows multiple minor peaks instead of a well-defined single peak. This is to be expected, as a larger opacity produces a stronger feedback with respect to the hydrogen only case, leading to multiple shocks in the gas. This complicate structure – i.e., a burst consisting of several sub-bursts – is commonly found (e.g., Ciotti & Ostriker 2007). In addition, the average accretion rate $\langle \lambda_{\rm rad} \rangle$ decreases from $\sim 3\%$ to $\sim 1\%$, but this can be understood by the increase of the mean temperature inside the Strömgren sphere to from $T_{\rm in} \sim 4 \times 10^4$ K to $\sim 6 \times 10^4$ K. The top panel of Figure 1 shows the accretion rate as a function of $\eta = 0.01$-0.1 with $M_{\rm bh} = 100~M_\odot$, $n_{\rm H,\infty} = 10^6$ cm^{-3}, and $T_\infty = 10^4$ K. Large symbols show $\langle \lambda_{\rm rad} \rangle$ while small symbols show $\lambda_{\rm rad,max}$. For the given set of parameters, the luminosity remains in the sub-Eddington regime, thus the effects of radiation pressures are minor. The bottom panel of Figure 1 shows the dependence of $\tau_{\rm cycle}$ on $\eta^{1/3}$, the same as found in Paper I. However, $\tau_{\rm cycle}$ for $\eta = 0.1$ is now ~ 2200 years which is $\sim 60\%$ of the value found in Paper I for the given set of parameters. This is also well understood (see Equation (22) in Paper I) as our model predicts $\tau_{\rm cycle} \propto \langle \lambda_{\rm rad} \rangle^{1/3}$.

3.1. Effect of Radiation Pressures

In Paper I, we have focused on exploring the parameter space in which the mean accretion rate is dominated by thermal feedback, i.e., radiation pressure can be neglected. We found $\langle \lambda_{\rm rad} \rangle \sim 1\%$ for $n_{\rm H,\infty} = 10^5$ cm^{-3}, assuming $M_{\rm bh} = 100~M_\odot$, $T_\infty = 10^4$ K, $\alpha = 1.5$, and including helium cooling/heating. However, not surprisingly, including the effect of radiation pressure produces a reduction of the accretion rate when the BH luminosity approaches the Eddington limit. Figure 2 shows $\langle \lambda_{\rm rad} \rangle$ as a function of gas density for a $100~M_\odot$ BH, comparing simulations that do not include radiation pressure (open triangles) to ones including pressure on H I only (open squares), on e^- only (open pentagons), and the total effect of radiation pressure (solid circles). Compton radiation pressure reduces the accretion rate below $\langle \lambda_{\rm rad} \rangle \sim 1\%$ for $n_{\rm H,\infty} \gtrsim 10^7$ cm^{-3} while the radiation pressure on H I appears always negligible with respect to Compton scattering. Both $\langle \lambda_{\rm rad} \rangle$ and $\lambda_{\rm rad,max}$ change from a constant fraction of the Bondi

accretion rate to the Eddington rate $\lambda_{\rm Edd}$, shown by the dashed line for $M_{\rm bh} = 100 \; M_\odot$ and radiative efficiency $\eta = 0.1$.

Figure 3 shows the dimensionless accretion rates $\langle \lambda_{\rm rad} \rangle$ and $\lambda_{\rm rad,max}$ as a function of the BH mass from $M_{\rm bh} = 10^2$ to $10^4 \; M_\odot$, keeping the other parameters constant: $\eta = 0.1$, $n_{\rm H,\infty} = 10^5$ cm^{-3}, and $T_\infty = 10^4$ K. The simulations include radiation pressures on H I and e^-, and show that the transition to Eddington-limited accretion happens for $M_{\rm bh} \simeq 5000 \; M_\odot$.

3.1.1. Transition from Bondi-like to Eddington-limited Accretion

So far the simulation results have shown that Compton scattering on electrons is the dominant radiation pressure effect, thus the Eddington-limit applies. Figure 4 summarizes the results of a large set of simulations that include radiation pressure. The top three panels in Figure 4(a) shows $\langle \lambda_{\rm rad} \rangle$ as a function of gas density for $M_{\rm bh} = 10^2, 10^3$, and $10^4 \; M_\odot$, respectively. For each BH mass, corresponding Eddington limits are shown by the dashed lines. The panels show the mean accretion rate $\langle \lambda_{\rm rad} \rangle$ (large triangles) and $\lambda_{\rm rad,max}$ (small triangles) transitioning from being a constant fraction of the Bondi rate at low densities to being Eddington-limited at higher densities. The period of the accretion $\tau_{\rm cycle}$, in the bottom panels, also shows different dependencies in Bondi-like and Eddington-limited regimes. We will come back to this in Section 3.2.

Figure 4(b) shows the mean accretion luminosity in units of $L_{\rm Edd}$ for $M_{\rm bh} = 10^2, 10^3$, and $10^4 \; M_\odot$ as a function of gas density. The dotted lines show 1% of the Bondi accretion rate for each BH mass. Thus, from Figure 4 approximately we have

$$\langle \dot{M} \rangle = \min(1\% T_{\infty,4}^{2.5} \dot{M}_B, \eta^{-1} \dot{M}_{\rm Edd}), \tag{6}$$

where $T_{\infty,4} \equiv T_\infty/(10^4 \text{ K})$, valid for density $n_{\rm H,\infty} \gtrsim 10^5$ cm^{-3}, and $\alpha = 1.5$.

It is thus apparent that IMBHs can grow at a rate near the Eddington limit if the gas density of the environment is larger than the critical density

$$n_{\rm H,\infty}^{\rm Edd} \sim 4 \times 10^6 \text{ cm}^{-3} \left(\frac{M_{\rm bh}}{10^2 \; M_\odot} \right)^{-1} \left(\frac{T_\infty}{10^4 \text{ K}} \right)^{-1} \left(\frac{\eta}{0.1} \right)^{-1}. \tag{7}$$

3.1.2. Why is Continuum Radiation Pressure Negligible?

As shown in Figure 2-4, the simulations show that radiation pressure on H I does not play an important role when the accretion rate is sub-Eddington. In this section, we focus on understanding why this is. Figure 5 shows the evolution of relative magnitude of acceleration due to radiation pressures normalized by the gravitational acceleration at a given radius. Each panel refers to a different density $n_{\rm H,\infty} = 10^5, 10^6, 10^7$, and 10^8 cm^{-3}. Within the Strömgren sphere, the relative effect of Compton radiation pressure remains constant as a function of the radius since the electron fraction x_{e^-} is close to unity

and the gas is nearly transparent to ionizing radiation. Outside of the Strömgren sphere, the rapid decrease of the electron fraction reduces the effect of Compton scattering. Radiation pressure on H I (thick lines in Figure 5) increases as a function of radius and has its peak value just inside the Strömgren sphere. This is due to the increase of the H I fraction as a function of radius. Outside the Strömgren sphere the relative effect of H I radiation pressure drops quickly because the ionizing luminosity decreases rapidly due to the increase of the H I opacity.

Continuum radiation pressure on H I is comparable to Compton electron scattering only in a shell just inside the Strömgren sphere, where the H I abundance starts to increase rapidly as a function of radius and the ionizing radiation is not fully shielded by H I. With increasing gas density, the peak and mean luminosities increase, hence the relative effect of Compton pressure on average increases and eventually becomes comparable to the effect of gravity (i.e., Eddington limit). Whereas Figure 5 shows that the relative effect of continuum radiation pressure does not increase much with increasing gas density. In addition, the range of variation of radiation pressures during a period of oscillation decreases with increasing density. In other words, at low densities radiation pressures display several magnitudes of variation which are not seen in the high-density regime. As a result, at low densities ($n_{\mathrm{H},\infty} \lesssim 10^6$ cm^{-3}) radiation pressure is significant only near the peaks of luminosity and generally is negligible compared to gravity; whereas at high densities ($n_{\mathrm{H},\infty} \gtrsim 10^7$ cm^{-3}) Compton scattering dominates throughout a period of oscillation reducing the accretion rate to Eddington-limited values. Only at intermediate densities $n_{\mathrm{H},\infty} \simeq 10^7$ cm^{-3}, the magnitude of H I radiation pressure just behind the Strömgren radius becomes comparable to that by Compton scattering.

The weak dependence of the H I radiation pressure on density and its magnitude with respect to the Compton pressure can be understood analytically. The key point is that the H I radiation pressure is proportional to the value of the neutral fraction $x_{\mathrm{H\,I}}$ just behind the Strömgren radius R_s and, assuming ionization equilibrium, it is easy to show that $x_{\mathrm{H\,I}}(R_s) \propto n_{\mathrm{H}}^{-2/3}$. It follows that the pressure on H I is relatively insensitive to variations of n_{H}:

$$P_{\mathrm{Rad}}^{\mathrm{cont}} \propto S_0 x_{\mathrm{H\,I}}(R_s) \exp\left[-\tau(R_s)\right] \propto n_{\mathrm{H}}^{1/3}, \tag{8}$$

where $S_0 \propto n_{\mathrm{H}}$ is the ionizing luminosity, and $\exp\left[-\tau(R_s)\right] = \mathrm{const}$. The derivation of $x_{\mathrm{H\,I}}(R_s)$ is as follows. At $R_s = S_0^{1/3} n_{\mathrm{H}}^{-2/3} \alpha_R^{-1/3}$ the photoionization rate is $\Gamma(R_s) = S_0 \sigma_{\mathrm{H\,I}}^{\mathrm{eff}}/4\pi R_s^2 \propto n_{\mathrm{H}}^{5/3}$. Assuming photoionization equilibrium $x_{\mathrm{H\,I}}(R_s)\Gamma(R_s) = n_{\mathrm{H}}\alpha_R$, we demonstrate that

$$x_{\mathrm{H\,I}}(R_s) = \frac{n_{\mathrm{H}}\alpha_R}{\Gamma(R_s)} \propto n_{\mathrm{H}}^{-2/3}. \tag{9}$$

3.2. Two Self-regulated Modes of Accretion: Collapsing I-front versus Quasi-steady I-front

One of the most interesting aspects of the radiation-regulated accretion onto BHs is the qualitative change of the period and duty cycle of the luminosity bursts observed in the high-density regime. As argued in Paper I and confirmed by further simulations in this work, the physical reason for this transition is a change of the dominant mechanism depleting the gas inside the Strömgren sphere between two consecutive

bursts. In the low-density regime, gas is pushed outward toward the ionization front by a pressure gradient (hereafter, mode-I accretion). At higher-densities gas accretion onto the BH becomes the dominant gas depletion mechanism (hereafter, mode-II accretion). Incidentally, as discussed below, simulations show that radiation pressure becomes important near the transition from mode-I to mode-II, at least for most of the initial conditions we have simulated. In Paper I, we have observed mode-II accretion only for our highest density simulation (for $n_{\rm H,\infty} = 10^7$ cm^{-3} and $M_{\rm bh} = 100$ $M_\odot$). In this paper, to better understand this regime, we have extended the parameter space to higher densities and higher BH masses. Figure 6 shows snapshots of the density (top halves in each panel) and ionization fraction (bottom halves in each panel) for two-dimensional simulations including radiation pressure, for $n_{\rm H,\infty} = 10^6$ cm^{-3} (top panels) and $n_{\rm H,\infty} = 10^7$ cm^{-3} (bottom panels). The snapshots are taken for each simulation at the moment of a burst of the accretion rate (left panels), in-between two bursts (middle panels), and just before a burst (right panels). For ambient density $n_{\rm H,\infty} = 10^6$ cm^{-3}, the Strömgren sphere collapses onto the BH which leads to a strong luminosity burst. On the contrary, the size of Strömgren sphere does not change much during the oscillation period for ambient density $n_{\rm H,\infty} = 10^7$ cm^{-3}. In this latter case, the oscillation of the accretion luminosity is driven by density and pressure waves originating at the I-front, while in the former case, the collapse of the I-front onto the BH leads to a much more intense accretion burst. In Figure 7(left), we compare the accretion rate onto the BH as a function of time for $n_{\rm H,\infty} = 10^6$ cm^{-3} (top panel) and $n_{\rm H,\infty} = 10^7$ cm^{-3} (bottom panel). For $n_{\rm H,\infty} = 10^6$ cm^{-3}, the collapse of I-front leads to strong burst of gas accretion, with $\lambda_{\rm rad,max}$ about $\times 20 \langle \lambda_{\rm rad} \rangle$. Hence, the duty cycle $f_{\rm duty}^{\rm I} \equiv \langle \lambda_{\rm rad} \rangle / \lambda_{\rm rad,max}$ is about 6%. The pressure gradient inside Strömgren sphere supports the gas shell accumulating at the I-front from collapsing until the accretion rate drops 4-5 orders of magnitude compared to the accretion during the burst. However, the Strömgren radius remains remarkably constant before its collapse due to the decline of gas density inside the H II region. In contrast, in the $n_{\rm H,\infty} = 10^7$ cm^{-3} simulation the accretion rate peaks at a few times $\langle \lambda_{\rm rad} \rangle$ before decreasing by about 2 orders of magnitude. The duty cycle approaches $f_{\rm duty}^{\rm II} \sim 50\%$ for this mode of accretion. As shown in Figures 3 and 4, simulations that do not include radiation pressure also show a rapid decrease of the period $\tau_{\rm cycle}$ and $\lambda_{\rm rad,max}$ with increasing gas density and BH mass, but the mean accretion rate $\langle \lambda_{\rm rad} \rangle$ does not. Thus, the reduced value of $\lambda_{\rm rad,max} / \langle \lambda_{\rm rad} \rangle \equiv 1/f_{\rm duty}^{\rm II}$ explains the longer duty cycle observed for mode-II accretion. A more detailed illustration of the qualitative difference between mode-I and mode-II accretion is shown in Figure 7(right). The figure shows the time evolution of the gas density profile (top panels), the temperature profile (middle panels) and the hydrogen ionization fraction (bottom panels) for the $n_{\rm H,\infty} = 10^6$ cm^{-3} and $n_{\rm H,\infty} = 10^7$ cm^{-3} simulations. Small variations of the density, temperature, and ionization fraction profiles are observed for $n_{\rm H,\infty} = 10^7$ cm^{-3}, while clear collapses of I-front are observed in the evolution of the profiles for $n_{\rm H,\infty} = 10^6$ cm^{-3}. Note that this quasi-stationary profile is not produced by the effects of radiation pressures. The same effect is found for $n_{\rm H,\infty} = 10^7$ cm^{-3} without including radiation pressure effects.

Interestingly, for our fiducial case simulations ($M_{\rm bh} = 100$ $M_\odot$, $T_\infty = 10^4$ K, $\eta = 0.1$, and $\alpha = 1.5$), the critical density at which the mean accretion rate becomes Eddington-limited nearly coincides with the critical density for transition from mode-I to mode-II accretion. This explains why the mean accretion rate and the peak accretion rate become Eddington-limited at nearly the same density. Indeed, if while increasing $n_{\rm H,\infty}$, the duty cycle remained at about 6% as in mode-I accretion, the mean accretion rate would not be

able to approach the Eddington limit, even though the peak accretion can be mildly super-Eddington. We will show below that the transition to mode-II accretion depends on the free parameters in the problem and may take place at much lower densities than the critical density for Eddington-limited accretion.

The quasi-stationary I-front observed for the $n_{\mathrm{H},\infty} = 10^7$ cm^{-3} simulation is also important to understand why there exists a clear transition to the Eddington-limited regime with increasing density or BH mass. For mode-I accretion, radiation pressure may become comparable to the gravity near the Strömgren radius, but this effect dominates only for a short time, during the peaks of luminosity. The peak accretion can indeed become moderately super-Eddington for a short time, also because of the broken spherical symmetry of the collapsing shell due to Rayleigh–Taylor instability of the accreting gas. However, for mode-II accretion, the geometry of accretion from large scales is quasi-spherical and radiation pressure effects are significant during the most of the duration of oscillations, hence the accretion rate is Eddington limited.

Figure 8 shows the relationship between the period of accretion bursts and the average size of the Strömgren sphere produced by the accreting BH. When the gas depletion inside the H II region is dominated by the outward flow of gas toward the I-front, $\tau_{\mathrm{cycle}}^{\mathrm{I}}$ shows a linear relation with $\langle R_s \rangle$ (solid line). This linear relation is almost identical to the results in Paper I, where helium cooling/heating was not included. By increasing the ambient gas density, eventually the gas depletion becomes dominated by accretion onto the BH. In this latter case, assuming that the dimensionless accretion rate $\langle \lambda_{\mathrm{rad}} \rangle$ is constant (a valid assumption in the sub-Eddington regime), τ_{cycle} scales as $\langle R_s \rangle^3$ (dotted line). However, the simulation results at high ambient gas density shown in Figure 8 are not well fitted by $\tau_{\mathrm{cycle}} \propto \langle R_s \rangle^3$, and indeed seem to follow a linear relationship $\tau_{\mathrm{cycle}} \propto \langle R_s \rangle$, similar to the low-density one but with an offset. This can be explained because at high densities the accretion rate becomes Eddington-limited soon after the transition to mode-II accretion for which $\tau_{\mathrm{cycle}} \propto \langle R_s \rangle^3$. It follows that the assumption $\langle \lambda_{\mathrm{rad}} \rangle \approx \mathrm{const}$ becomes invalid and instead $\tau_{\mathrm{cycle}}^{\mathrm{II}} \equiv t_{\mathrm{in}} \propto \rho \langle R_s \rangle^3 / \dot{M}_{\mathrm{Edd}}$. In this regime, since the Strömgren radius is $\langle R_s \rangle^3 \propto \eta \dot{M}_{\mathrm{Edd}}/\rho^2$, we get $\rho \propto \dot{M}_{\mathrm{Edd}}^{1/2} \langle R_s \rangle^{-1.5}$ and

$$\tau_{\mathrm{cycle}}^{\mathrm{II}} \propto M_{\mathrm{bh}}^{-0.5} \langle R_s \rangle^{1.5}. \tag{10}$$

As shown by the dashed lines in Figure 8, this model is in good agreement with the results of the simulations for different values of M_{bh}.

Thus, the small offset in τ_{cycle} observed in Figure 8 when the density is increased, can be understood because $n_{\mathrm{H},\infty}^{\mathrm{cr}}$, at which the transition from mode-I to mode-II accretion takes place, is nearly equal to $n_{\mathrm{H},\infty}^{\mathrm{Edd}}$, the critical density at which the mean accretion rate becomes Eddington limited. But, in general, the ratio of these critical densities may depend on all the free parameters of the model.

Our analytical model of feedback-regulated feeding of the BH, can help understand the dependence of the critical density on all the parameter space, not fully covered by the simulations. We found that the cycle period τ_{cycle} is the shortest time between the gas depletion timescales $t_{\mathrm{in}} = M_{\mathrm{H\,II}}/\dot{M}$, where $M_{\mathrm{H\,II}} \sim \rho_{\mathrm{in}} \langle R_s \rangle^3$ is the mass inside the H II region, and $t_{\mathrm{out}} \approx 3\langle R_s \rangle / c_{\mathrm{s,in}}$ (see Paper I). Thus, by definition, when the density approaches the critical density we have $t_{\mathrm{in}} \simeq t_{\mathrm{out}}$, but this condition also implies that the mean Strömgren radius approaches the effective accretion radius:

$$\langle R_s \rangle^{\mathrm{cr}} \approx 10 \times r_{\mathrm{b,eff}}. \tag{11}$$

Equation (11), is derived setting $\dot{M} = \langle \dot{M} \rangle \equiv 4\pi\rho_{\mathrm{in}}c_{\mathrm{s,in}}r_{\mathrm{b,eff}}^2 \equiv \langle \lambda_{\mathrm{rad}} \rangle \dot{M}_B$ in the relationship for t_{in}. Since in our model we have $\rho_{\mathrm{in}}T_{\mathrm{in}} \simeq \rho_\infty T_\infty$, it follows that $r_{\mathrm{b,eff}} \approx (T_{\mathrm{in}}/T_\infty)^{1/4}\langle \lambda_{\mathrm{rad}} \rangle^{1/2}r_{\mathrm{b}}$, and $\langle R_s \rangle^{\mathrm{cr}} \simeq 2T_{\infty,4}T_{\mathrm{in},*}^{-7/4}r_{\mathrm{b}}$, where $r_{\mathrm{b}} \equiv GM/c_{s,\infty}^2$ is the Bondi radius, $T_{\infty,4} \equiv T_\infty/10^4$ K, and $T_{\mathrm{in},*} \equiv T_{\mathrm{in}}/6 \times 10^4$ K is the mean temperature at the accretion radius inside the H II region (normalized to the value found for $\alpha = 1.5$). Thus, $\langle R_s \rangle^{\mathrm{cr}}$ and period of the bursts are

$$\langle R_s \rangle^{\mathrm{cr}} \approx (0.01\ \mathrm{pc})M_{\mathrm{bh},2}T_{\mathrm{in},*}^{-7/4}, \tag{12}$$

$$\tau_{\mathrm{cycle}}^{\mathrm{cr}} \approx (1000\ \mathrm{yr})M_{\mathrm{bh},2}T_{\mathrm{in},*}^{-9/4}, \tag{13}$$

with $M_{\mathrm{bh},2} \equiv M_{\mathrm{bh}}/100\ M_\odot$.

Applying naively the analytical expression for the Strömgren radius produced by a source of luminosity $L \equiv \eta c^2 \langle \dot{M} \rangle$ in a gas of density ρ_∞ gives $\langle R_s \rangle \propto M^{2/3}n_{\mathrm{H},\infty}^{-1/3}T_\infty^{1/3}\eta^{1/3}$. However, using the simulation data, we find that the mean radius of the Strömgren sphere in the sub-Eddington regime is nearly independent of T_∞, and if $\langle R_s \rangle \sim \langle R_s \rangle^{\mathrm{cr}}$, is also independent of η:

$$\langle R_s \rangle \approx (0.015\ \mathrm{pc})M_{\mathrm{bh},2}^{2/3} \left(\frac{n_{\mathrm{H},\infty}}{10^6\ \mathrm{cm}^{-3}} \right)^{-1/3} \left(\frac{\bar{E}}{41\ \mathrm{eV}} \right)^{-5/8}, \tag{14}$$

where $\bar{E} \equiv L_0/S_0$ is the mean energy of ionizing photons, and we have assumed hydrogen recombination coefficient $\alpha_R = (4 \times 10^{13}\ \mathrm{cm}^3/\mathrm{s})T_{\mathrm{in},*}^{-1/2}$. In addition, we find that, $\langle R_s \rangle \propto \eta^{1/3}$ as expected for $\langle R_s \rangle \gg \langle R_s \rangle^{\mathrm{cr}}$. The deviation from the naive expectation is not surprising, as the BH luminosity and the density inside the Strömgren sphere are not constant with time. Indeed, although both the maximum and mean luminosities of the BH are $\propto \eta$, the simulations show that the luminosity at the minimum of the cycle, L^{min}, is nearly independent of η. Typically $L^{\mathrm{min}} \ll L$, but when $n_{\mathrm{H},\infty}$ approaches the critical value $L^{\mathrm{min}} \sim L$. Similarly, assuming an effective mean density $(\rho_{\mathrm{in}}\rho_\infty)^{1/2}$ in the Strömgren radius expression would explain the temperature dependence in Equation (14).

Finally, setting $\langle R_s \rangle = \langle R_s \rangle^{\mathrm{cr}}$ we derive the critical density

$$n_{\mathrm{H},\infty}^{\mathrm{cr}} \sim (5 \times 10^6\ \mathrm{cm}^{-3})M_{\mathrm{bh},2}^{-1}T_{\mathrm{in},*}^{7/4} \left(\frac{\bar{E}}{41\ \mathrm{eV}} \right)^{-1}. \tag{15}$$

The critical density $n_{\mathrm{H},\infty}^{\mathrm{cr}}$ as well as other scaling relationships in our model depends on $\bar{E} \equiv L/S_0$ and T_{in}, but for a gas of zero metallicity (including helium), these quantities are determined only by the spectrum of the radiation. Assuming a power law spectrum with index α is easy to show that

$$\bar{E} = 13.6\ \mathrm{eV} \begin{cases} \alpha/(\alpha - 1) & \text{if } \alpha > 1, \\ \ln(h\nu_{\mathrm{max}}/13.6\ \mathrm{eV}) & \text{if } \alpha = 1 \\ \alpha/(1 - \alpha)(h\nu_{\mathrm{max}}/13.6\ \mathrm{eV})^\alpha & \text{if } \alpha < 1. \end{cases} \tag{16}$$

We have estimated $h\nu_{\mathrm{max}} = 0.2$ keV as the frequency at which the mean free path of the photons equals $\langle R_s \rangle$. The points in Figure 9 show T_{in} as a function of $\bar{E}$ for simulations with $\alpha = 0.5, 1, 1.5, 2, 2.5$ taken

from Figure 9 in Paper I. The line shows the fit to the points:

$$T_{\mathrm{in},*} \approx \left(\frac{\bar{E}}{41 \text{ eV}} \right)^{1/4}.$$ (17)

For our fiducial model, for which $\bar{E} \sim 41$ eV, the value of the critical density is very close to $n_{\mathrm{H},\infty}^{\mathrm{Edd}}$ given in Equation (7):

$$\frac{n_{\mathrm{H},\infty}^{\mathrm{cr}}}{n_{\mathrm{H},\infty}^{\mathrm{Edd}}} \approx \eta_{-1} T_{\infty,4} \left(\frac{\bar{E}}{41 \text{ eV}} \right)^{-9/16}.$$ (18)

From an inspection of Equation (18) is evident that the only cases in which $n_{\mathrm{H},\infty}^{\mathrm{cr}}$ can be larger than $n_{\mathrm{H},\infty}^{\mathrm{Edd}}$ are assuming the largest realistic values of unity for $T_{\infty,4}$ and η_{-1}, and assuming a spectrum of radiation from the BH softer than $\alpha = 1.5$ that would reduce $\bar{E}$ with respect to the fiducial value. Vice versa a hard spectrum, low radiative efficiency and accretion from a gas colder than 10^4 K would decrease the ratio $n_{\mathrm{H},\infty}^{\mathrm{cr}}/n_{\mathrm{H},\infty}^{\mathrm{Edd}}$ below unity, making mode-II accretion sub-Eddington for a wider range of densities. For these cases the period of the cycle could become very short with increasing density as $\tau_{\mathrm{cycle}} \propto \langle R_s \rangle^3 \propto n_{\mathrm{H},\infty}^{-1}$.

3.3. Effect of Non-zero Angular Momentum of Gas

As discussed in Paper I, the introduction of small angular momentum in the flow, which is realistic in most astrophysical problems, can modify the time-dependent behavior of accretion rate presented in this series of papers. Angular momentum of gas leads to the formation of an accretion disk near the Schwartzshild radius of a BH. This disk is not resolved in our simulations. Thus, the accreted gas may experience a time delay before it is converted to radiation. Here, we test how the introduction of time delay would affect the feedback loops of accretion.

As mentioned in Section 2, it is important to estimate physically motivated time delays. Here, we explore the time delay of 1–300 times $t_{\mathrm{ff}}(R_{\mathrm{min}})$ which is large enough with an assumption of α-disk model. On the other hand, no matter how long is the time delay, what really matters is how the time delay compares to the oscillation period, which depends mainly on the gas density for a fixed mass of BH. We investigate this issue in the low ($n_{\mathrm{H},\infty} = 10^5$ cm^{-3}) and high density ($n_{\mathrm{H},\infty} = 10^7$ cm^{-3}) regimes where the oscillation pattern and the periods are different. At low densities a time delay of a few hundred free-fall times is much smaller compared to the oscillation period, whereas at high densities the maximum time delay that we have tested is comparable to the oscillation period. In the left panel of Figure 10 which shows the result for $n_{\mathrm{H},\infty} = 10^5$ cm^{-3}, τ_{cycle} does not increase at all as a function of time delay since the introduced time delay is much smaller than the original oscillation period. In the right panel of Figure 10 for $n_{\mathrm{H},\infty} = 10^7$ cm^{-3}, the maximum time delay that we introduce is comparable to the original oscillation period, and we see that τ_{cycle} increase approximately by the amount of time delay. In both cases, we still observe oscillations. Thus, only in the case of accretion from a high-density gas which produces shorter oscillation period, and for an accretion disk with $R_{\mathrm{disk}} \sim R_{\mathrm{min}}$, the time delay may have an important effect on the accretion rate.

Indeed, the accretion disk may not only introduce a time delay but also smooth out the accretion rate on a timescale of the order of the viscous timescale. In this case for cases in which the disk is large ($R_{\mathrm{disk}} \sim$

R_{min}) and τ_{cycle} is short (i.e., for mode-II accretion), the disk may further smooth out or completely erase the periodic low-amplitude oscillations in the accretion rate from large scales.

4.   Summary and Discussion: Scaling Relationships

We have presented a systematic study on how the classic Bondi problem of spherical accretion onto a compact object is modified by the effects of radiation feedback. We solve radiative transfer equations in the radial direction for the hydrogen and helium ionizing radiation emitted by the BH. Gas is optically thin inside Strömgren radius while it becomes optically thick for gas outside the ionized gas. In this paper, the second of a series, we have focused on the effects that radiation pressure and angular momentum have on the gas supply and accretion rate onto the BH. The simulations focused on accretion onto IMBHs but the analytical scaling relationships we have derived are rather general, and although the initial conditions are somewhat idealized, should describe reality more accurately than the classical Bondi formulae.

Here, we summarize the main results and scaling relationships we found in the first two papers of this series for non-moving BHs accreting from a uniform medium. In our models we have assumed that the BH accretes from a uniform density and temperature reservoir, significantly larger than the Bondi radius and $\langle R_s \rangle$. This assumption is well motivated for accretion onto stellar and IMBH, but for SMBH there could be supply of gas to the BH from stars within $\langle R_s \rangle$ (stellar winds) or other astrophysical object (merger-driven accretion, etc). The scaling relationships can be applied to problems involving a wide range of masses of the accretor, from stellar mass objects (e.g., Wheeler & Johnson 2011) to supermassive BHs. One caveat is that we are neglecting the effects of self-gravity of the gas (see Li 2011) and the gravitational potential due to the dark matter halo of the host galaxy, which may play an important role for the case of accretion onto supermassive BHs. Indeed, a simple calculation shows that at the I-front gravity due to the mass of the gas inside the Strömgren sphere exceeds the BH's gravity if $M_{\text{bh}} \gtrsim 10^6 \, M_\odot/(\eta_{-1} T_{\infty,4})$. Our model predicts scaling relationships for the period, duty cycle, peak and mean accretion onto the BH, as well as relevant critical densities and size of the Strömgren sphere around the BH. In the following summary of the scaling relationships, we express T_{in} in the equations in terms of $\bar{E}$ given by Equation (17) that is valid for a gas of low-metallicity. $\bar{E}$ is related to the spectral index α by Equation (16). For higher values of the gas metallicity, the coefficients in the equations can be different due to changes in the relationship between T_{in} and the spectrum of the radiation. A caveat is that our simulations have explored a large but limited parameter space for the masses of the BHs, temperature and density of the ambient gas, etc. So, the proposed scaling relationships, although they are based on a physically motivated model we inferred from the simulations, should be used with caution for sets of parameters that are significantly different from the range confirmed by simulations.

The main qualitative result of our study is that radiation feedback produces periodic oscillations of the accretion rate from large scales onto the BH, and thus periodic short-lived bursts of the BH luminosity. We

found two modes of self-regulated accretion, determined by

$$n_{\rm H,\infty}^{\rm cr} \sim \frac{5 \times 10^6 \ {\rm cm}^{-3}}{M_{\rm bh,2}} \left(\frac{\bar{E}}{41 \ {\rm eV}}\right)^{-9/16}. \tag{19}$$

If $n_{\rm H,\infty} < n_{\rm H,\infty}^{\rm cr}$ (mode-I), the accretion luminosity of the BH has regular bursts with period $\tau_{\rm cycle}^{\rm I}$ during which the BH increases its brightness by about 5 orders of magnitude but only for a short fraction of the cycle period: the duty cycle is $f_{\rm duty}^{\rm I} \equiv \tau_{\rm on}/\tau_{\rm cycle} \sim 6\% \ T_{\infty,4}^{1/2}$. During the quiescent phase in the accretion cycle the gas accumulates in a dense shell in front of the H II region rather than accreting directly onto the BH. As the luminosity decreases after the burst, the density inside the H II region also decreases because is pushed outward by a pressure gradient, thus maintaining the I-front radius nearly constant. Eventually the density and pressure inside the H II region cannot sustain the weight of the dense shell that collapses producing a burst of accretion. The cycle repeats regularly. If $n_{\rm H,\infty} > n_{\rm H,\infty}^{\rm cr}$ (mode-II) the cycle is qualitatively different: the duty cycle is about $f_{\rm duty}^{\rm II} \gtrsim 50\%$ and the peak accretion rate is only a few times the mean. There is no collapse phase of the dense shell and the H II region remains roughly stationary while the accretion rate oscillates. The physical motivation for mode-II accretion is that the timescale for the depletion of the gas inside the H II region becomes dominated by accretion onto the BH. Only for mode-II accretion the BH growth rate can approach the Eddington limit, given that the density exceeds the critical density

$$n_{\rm H,\infty}^{\rm Edd} \sim \frac{4 \times 10^6 \ {\rm cm}^{-3}}{M_{\rm bh,2}} T_{\infty,4}^{-1} \eta_{-1}^{-1}. \tag{20}$$

For nearly all realistic cases $n_{\rm H,\infty}^{\rm Edd} \gtrsim n_{\rm H,\infty}^{\rm cr}$.

For $M_{\rm bh} = 100 \ M_\odot$, at densities $10^5 \ {\rm cm}^{-3} \le n_{\rm H,\infty} \le n_{\rm H,\infty}^{\rm Edd}$ the *mean accretion rate* onto the BH, in units of the Bondi rate is $\langle\lambda_{\rm rad}\rangle \sim 1\% T_{\infty,4}^{2.5}(\bar{E}/41 \ {\rm eV})^{-1}$, independent of all the other parameters. For $n_{\rm H,\infty} < 10^5 \ {\rm cm}^{-3}$ instead, $\langle\lambda_{\rm rad}\rangle \sim 1\%(n_{\rm H,\infty}/10^5 \ {\rm cm}^{-3})^{1/2}T_{\infty,4}^{2.5}(\bar{E}/41 \ {\rm eV})^{-1}$, depends weakly on the gas density. One caveat is that in Paper I the dependence on the free parameters of the transition density $n_{\rm H,\infty} = 10^5 \ {\rm cm}^{-3}$ has been only partially explored. As shown in Figure 4 of the present paper, the simulation results are consistent with a transition density inversely proportional to the BH mass. Hence, if $10^5 M_{\rm bh,2}^{-1} \ {\rm cm}^{-3} \le n_{\rm H,\infty} \le n_{\rm H,\infty}^{\rm Edd}$ the mean accretion rate is proportional to the thermal pressure $n_{\rm H,\infty}T_\infty$ of the ambient gas:

$$\langle\dot{M}\rangle \approx (4 \times 10^{18} \ {\rm g \ s}^{-1})M_{\rm bh,2}^2 \left(\frac{n_{\rm H,\infty}}{10^5 \ {\rm cm}^{-3}}\right) T_{\infty,4} \left(\frac{\bar{E}}{41 \ {\rm eV}}\right)^{-1}. \tag{21}$$

If $n_{\rm H,\infty} > n_{\rm H,\infty}^{\rm Edd}$ then $\langle\dot{M}\rangle = L_{\rm Edd}(\eta c^2)^{-1}$. The duty cycle is

$$f_{\rm duty} = \begin{cases} f_{\rm duty}^{\rm I} \approx 6\% T_{\infty,4}^{1/2} & {\rm if} \ n_{\rm H,\infty} \le n_{\rm H,\infty}^{\rm cr} \\ f_{\rm duty}^{\rm II} \gtrsim 50\% & {\rm if} \ n_{\rm H,\infty} > n_{\rm H,\infty}^{\rm cr}, \end{cases} \tag{22}$$

and the maximum accretion luminosity which depends on the duty cycle thus is,

$$\frac{L^{\rm max}}{L_{\rm Edd}} \approx \min\left[1, \mathcal{A}\eta_{-1}M_{\rm bh,2} \left(\frac{n_{\rm H,\infty}}{10^5 \ {\rm cm}^{-3}}\right) T_{\infty,4} \left(\frac{\bar{E}}{41 \ {\rm eV}}\right)^{-1}\right], \tag{23}$$

where $L_{\rm Edd} = 1.3 \times 10^{40} M_{\rm bh,2}$ erg s^{-1}, and

$$\mathcal{A} = \begin{cases} \mathcal{A}^{\rm I} \approx 0.5\, T_{\infty,4}^{-1/2} & \text{if } n_{\rm H,\infty} \leq n_{\rm H,\infty}^{\rm cr} \\ \mathcal{A}^{\rm II} \approx 0.06 & \text{if } n_{\rm H,\infty} > n_{\rm H,\infty}^{\rm cr} \end{cases} \tag{24}$$

The cycle of the oscillations also falls into two regimes:

$$\tau_{\rm cycle} = \begin{cases} \tau_{\rm cycle}^{\rm I} \approx (0.1\,{\rm Myr})\, M_{\rm bh,2}^{2/3} \eta_{-1}^{1/3} (\frac{n_{\rm H,\infty}}{1\,{\rm cm}^{-3}})^{-1/3} (\frac{\bar{E}}{41\,{\rm eV}})^{-3/4}, & \text{if } n_{\rm H,\infty} \leq n_{\rm H,\infty}^{\rm cr} \\ \tau_{\rm cycle}^{\rm II} \approx (1\,{\rm Gyr})\, \eta_{-1} (\frac{n_{\rm H,\infty}}{1\,{\rm cm}^{-3}})^{-1} (\frac{\bar{E}}{41\,{\rm eV}})^{-7/8}, & \text{if } n_{\rm H,\infty} > n_{\rm H,\infty}^{\rm cr}. \end{cases} \tag{25}$$

The astrophysical applications of this model are innumerable and are beyond the aim of this paper to discuss them in detail. However, one of the most obvious results is that the luminosity of an accreting BH should be smaller than the value inferred applying the Bondi formula. Not only because the mean accretion rate is always $\lesssim 1\%$ of the Bondi rate, but also because if $n_{\rm H,\infty} < n_{\rm H,\infty}^{\rm cr}$, 94% of the time is about 5 orders of magnitude lower than the Bondi rate inferred from the ambient medium temperature and density. Thus, this simple arguments could have interesting consequences to interpret the observed quiescence of SMBH in ellipticals and Sgr A*. Also, the duty cycle of $\sim 6\%\, T_{\infty,4}^{1/2}$ we found for mode-I accretion is interestingly close to the fraction of galaxies with AGNs $\sim 3\%$ found deep field surveys (e.g., Steidel et al. 2002; Luo et al. 2011). For SMBHs of about $10^6\, M_\odot$, $n_{\rm H,\infty}^{\rm cr} \sim 500\, {\rm cm}^{-3}$.

In this paper we also found that IMBH can grow at near the Eddington limit if $n_{\rm H,\infty} > \max(n_{\rm H,\infty}^{\rm Edd}, n_{\rm H,\infty}^{\rm cr})$. This has potentially important consequences on the ability of seed IMBH from Population III stars to grow by accretion into SMBH during the first gigayears of the universe age. This possibility seemed precluded if the duty cycle of the burst was 6% as found in previous works.

Finally, although the nature of ULXs is unknown, there are indications that they may host an IMBH (e.g., Strohmayer & Mushotzky 2009). An IMBH accreting from an interstellar medium (ISM) with high pressure such as dense molecular cloud ($n_{\rm H,\infty} T_\infty \sim 10^5$–$10^7\, {\rm cm}^{-3}$ K) would be $L^{\rm max} \sim 10^{37}$–10^{39} erg s^{-1} for $M_{\rm bh} = 1000\, M_\odot$, that is comparable to the luminosity of ULXs. However, this assumes that the IMBH is at rest with respect to the ISM. We will focus on gas accretion onto moving BHs with radiation feedback in the third paper of this series (K. Park & M. Ricotti 2012, in preparation). Clearly, more work is needed to address each of the aforementioned topics in detail, but the basic ground work presented in the present paper may allow the re-visitation of a few longstanding problems still unsolved in astrophysics.

REFERENCES

Abel, T., Anninos, P., Norman, M. L., & Zhang, Y. 1998, ApJ, 508, 518

Abel, T., Bryan, G. L., & Norman, M. L. 2000, ApJ, 540, 39

Alvarez, M. A., Wise, J. H., & Abel, T. 2009, ApJ, 701, L133

Begelman, M. C. 1985, ApJ, 297, 492

Begelman, M. C., Volonteri, M., & Rees, M. J. 2006, MNRAS, 370, 289

Bisnovatyi-Kogan, G. S., & Blinnikov, S. I. 1980, MNRAS, 191, 711

Bondi, H. 1952, MNRAS, 112, 195

Bondi, H., & Hoyle, F. 1944, MNRAS, 104, 273

Bromm, V., Coppi, P. S., & Larson, R. B. 1999, ApJ, 527, L5

Carr, B. J., Bond, J. R., & Arnett, W. D. 1984, ApJ, 277, 445

Ciotti, L., & Ostriker, J. P. 2007, ApJ, 665, 1038

Ciotti, L., Ostriker, J. P., & Proga, D. 2009, ApJ, 699, 89

Cowie, L. L., Ostriker, J. P., & Stark, A. A. 1978, ApJ, 226, 1041

Di Matteo, T., Colberg, J., Springel, V., Hernquist, L., & Sijacki, D. 2008, ApJ, 676, 33

Fryer, C. L., Woosley, S. E., & Heger, A. 2001, ApJ, 550, 372

Greif, T. H., Johnson, J. L., Klessen, R. S., & Bromm, V. 2008, MNRAS, 387, 1021

Haehnelt, M. G., Natarajan, P., & Rees, M. J. 1998, MNRAS, 300, 817

Hayes, J. C., Norman, M. L., Fiedler, R. A., Bordner, J. O., Li, P. S., Clark, S. E., ud-Doula, A., & Mac
    Low, M.-M. 2006, ApJS, 165, 188

Johnson, J. L., & Bromm, V. 2007, MNRAS, 374, 1557

Johnson, J. L., Khochfar, S., Greif, T. H., & Durier, F. 2011, MNRAS, 410, 919

Kim, J.-h., Wise, J. H., Alvarez, M. A., & Abel, T. 2011, ApJ, 738, 54

Krolik, J. H. 2004, ApJ, 615, 383

Krolik, J. H., & Kallman, T. R. 1984, ApJ, 286, 366

Krolik, J. H., & London, R. A. 1983, ApJ, 267, 18

Krolik, J. H., McKee, C. F., & Tarter, C. B. 1981, ApJ, 249, 422

Kurosawa, R., & Proga, D. 2009a, MNRAS, 397, 1791

—. 2009b, ApJ, 693, 1929

Kurosawa, R., Proga, D., & Nagamine, K. 2009, ApJ, 707, 823

Li, Y. 2011, ArXiv e-prints

Luo, B., et al. 2011, ApJ, 740, 37

Lusso, E., & Ciotti, L. 2011, A&A, 525, A115

Mack, K. J., Ostriker, J. P., & Ricotti, M. 2007, ApJ, 665, 1277

Madau, P., & Rees, M. J. 2001, ApJ, 551, L27

Mayer, L., Kazantzidis, S., Escala, A., & Callegari, S. 2010, Nature, 466, 1082

Miller, M. C., & Colbert, E. J. M. 2004, International Journal of Modern Physics D, 13, 1

Milosavljević, M., Bromm, V., Couch, S. M., & Oh, S. P. 2009a, ApJ, 698, 766

Milosavljević, M., Couch, S. M., & Bromm, V. 2009b, ApJ, 696, L146

Novak, G. S., Ostriker, J. P., & Ciotti, L. 2011, ApJ, 737, 26

Oh, S. P., & Haiman, Z. 2002, ApJ, 569, 558

Omukai, K., Schneider, R., & Haiman, Z. 2008, ApJ, 686, 801

Ostriker, J. P., Choi, E., Ciotti, L., Novak, G. S., & Proga, D. 2010, ApJ, 722, 642

Ostriker, J. P., Weaver, R., Yahil, A., & McCray, R. 1976, ApJ, 208, L61

Park, K., & Ricotti, M. 2011, ApJ, 739, 2

Pelupessy, F. I., Di Matteo, T., & Ciardi, B. 2007, ApJ, 665, 107

Proga, D. 2007, ApJ, 661, 693

Proga, D., Ostriker, J. P., & Kurosawa, R. 2008, ApJ, 676, 101

Regan, J. A., & Haehnelt, M. G. 2009, MNRAS, 396, 343

Ricotti, M. 2007, ApJ, 662, 53

—. 2009, MNRAS, 392, L45

Ricotti, M., Gnedin, N. Y., & Shull, J. M. 2001, ApJ, 560, 580

Ricotti, M., & Ostriker, J. P. 2004, MNRAS, 352, 547

Ricotti, M., Ostriker, J. P., & Gnedin, N. Y. 2005, MNRAS, 357, 207

Ricotti, M., Ostriker, J. P., & Mack, K. J. 2008, ApJ, 680, 829

Sazonov, S. Y., Ostriker, J. P., Ciotti, L., & Sunyaev, R. A. 2005, MNRAS, 358, 168

Schneider, R., Ferrara, A., Natarajan, P., & Omukai, K. 2002, ApJ, 571, 30

Shakura, N. I., & Sunyaev, R. A. 1973, A&A, 24, 337

Shapiro, S. L. 1973, ApJ, 180, 531

Steidel, C. C., Hunt, M. P., Shapley, A. E., Adelberger, K. L., Pettini, M., Dickinson, M., & Giavalisco, M. 2002, ApJ, 576, 653

Stone, J. M., & Norman, M. L. 1992, ApJS, 80, 753

Strohmayer, T. E., & Mushotzky, R. F. 2009, ApJ, 703, 1386

van der Marel, R. P. 2004, Coevolution of Black Holes and Galaxies, 37

Vitello, P. 1984, ApJ, 284, 394

Volonteri, M., Haardt, F., & Madau, P. 2003, ApJ, 582, 559

Volonteri, M., Lodato, G., & Natarajan, P. 2008, MNRAS, 383, 1079

Volonteri, M., & Rees, M. J. 2005, ApJ, 633, 624

Wandel, A., Yahil, A., & Milgrom, M. 1984, ApJ, 282, 53

Wheeler, J. C., & Johnson, V. 2011, ApJ, 738, 163

Yoo, J., & Miralda-Escudé, J. 2004, ApJ, 614, L25
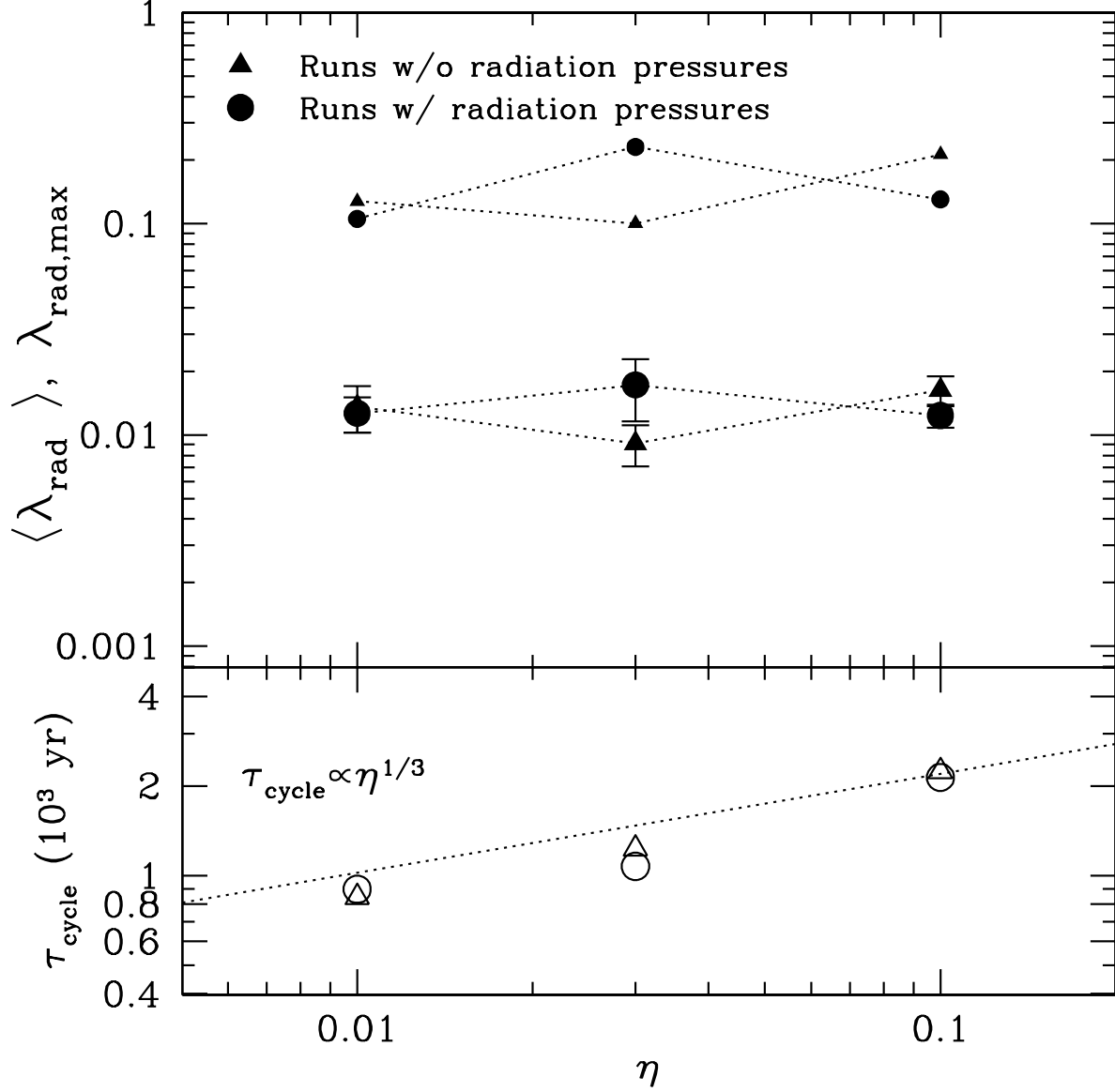
Fig. 1.— Top: accretion rate in units of the Bondi rate as a function of radiative efficiency η for simulations with $M_{bh} = 100\ M_\odot$, $n_{H,\infty} = 10^6\ cm^{-3}$, and $T_\infty = 10^4$ K. Large symbols indicate mean accretion rate ($\langle\lambda_{rad}\rangle \sim 1\%$), while small symbols show accretion rate at peaks ($\lambda_{rad,max} \sim 20\%$). Bottom: period between bursts τ_{cycle} as a function η. The dotted line shows $\tau_{cycle} \propto \eta^{1/3}$. In both panels, triangles represent simulations neglecting the effect of radiation pressures, while circles show simulations including radiation pressures. Radiation pressures introduce a minor difference in both the accretion rate and period of the bursts for this parameter set.
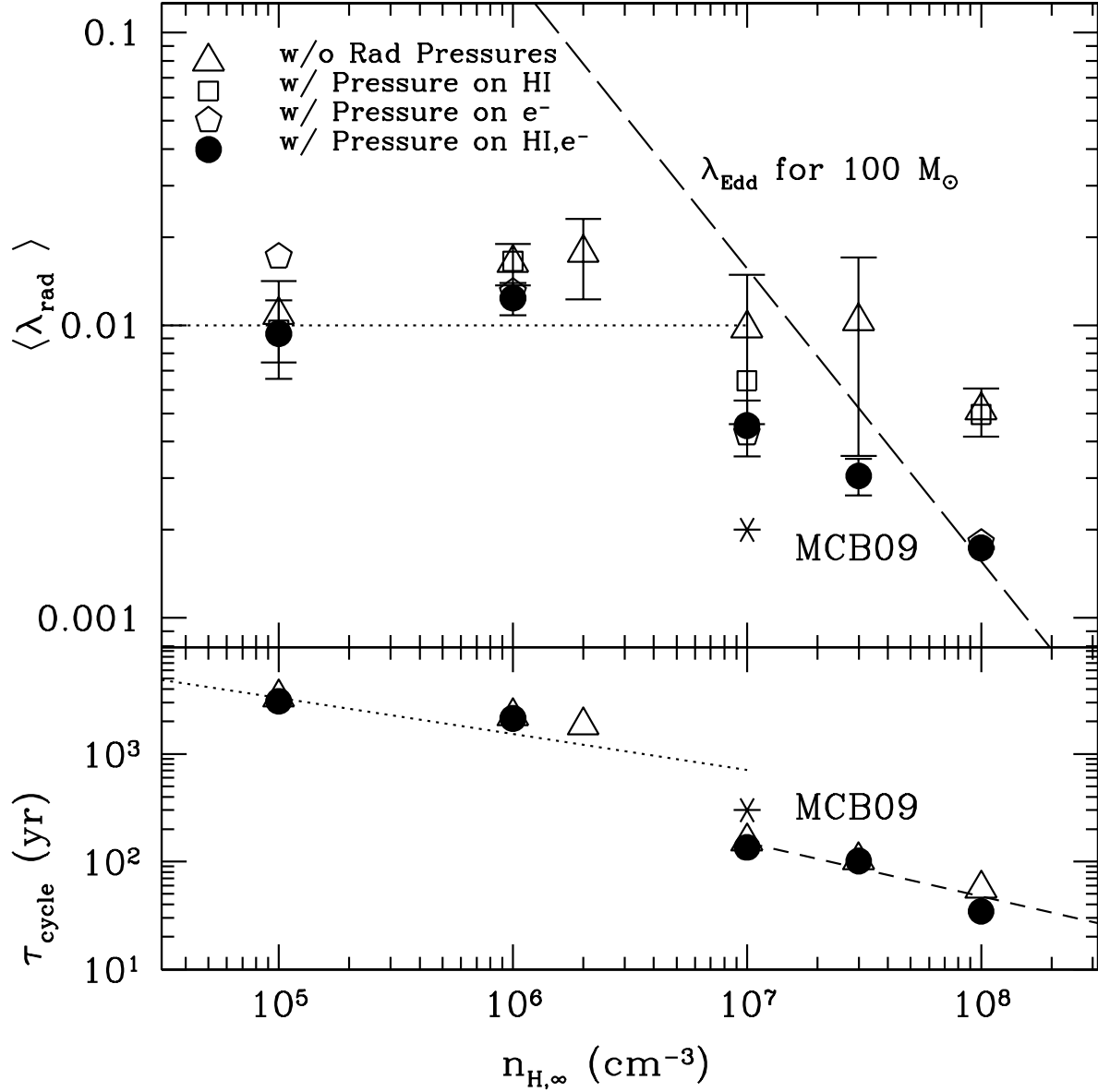
Fig. 2.— Comparison of relative importance of radiation pressures in regulating mean accretion rate (top panel) and the period of bursts (bottom panel) as a function of the ambient gas density $n_{H,\infty}$. Symbols are explained in the legend of the figure. Top: long dashed line shows the Eddington limit for a 100 $M_\odot$ BH with $\eta = 0.1$. When the accretion rate is sub-Eddington ($n_{H,\infty} \leq 10^6$ cm^{-3}) radiation pressures both on electrons and H I do not play an important role and the thermal structure of the Strömgren sphere regulates the accretion. Radiation pressure is important in reducing the accretion rate at $n_{H,\infty} = 10^7$ cm^{-3} where the accretion rate approaches the Eddington rate. The transition of accretion rate from $\langle\lambda_{rad}\rangle \sim 1\%$ to the Eddington-limited regime happens at $n_{H,\infty}^{Edd} \sim 4 \times 10^6$ cm^{-3} for a 100 $M_\odot$ BH with $\eta = 0.1$ and $T_\infty = 10^4$ K. Bottom: radiation pressures do not produce significant differences in τ_{cycle}. Transition of τ_{cycle} from mode-I (dotted line) to mode-II (short dashed line) happens at the critical density $n_{H,\infty}^{cr} \sim n_{H,\infty}^{Edd}$ (see Section 3.2). The result shows a good agreement with the work of Milosavljević et al. (2009b)
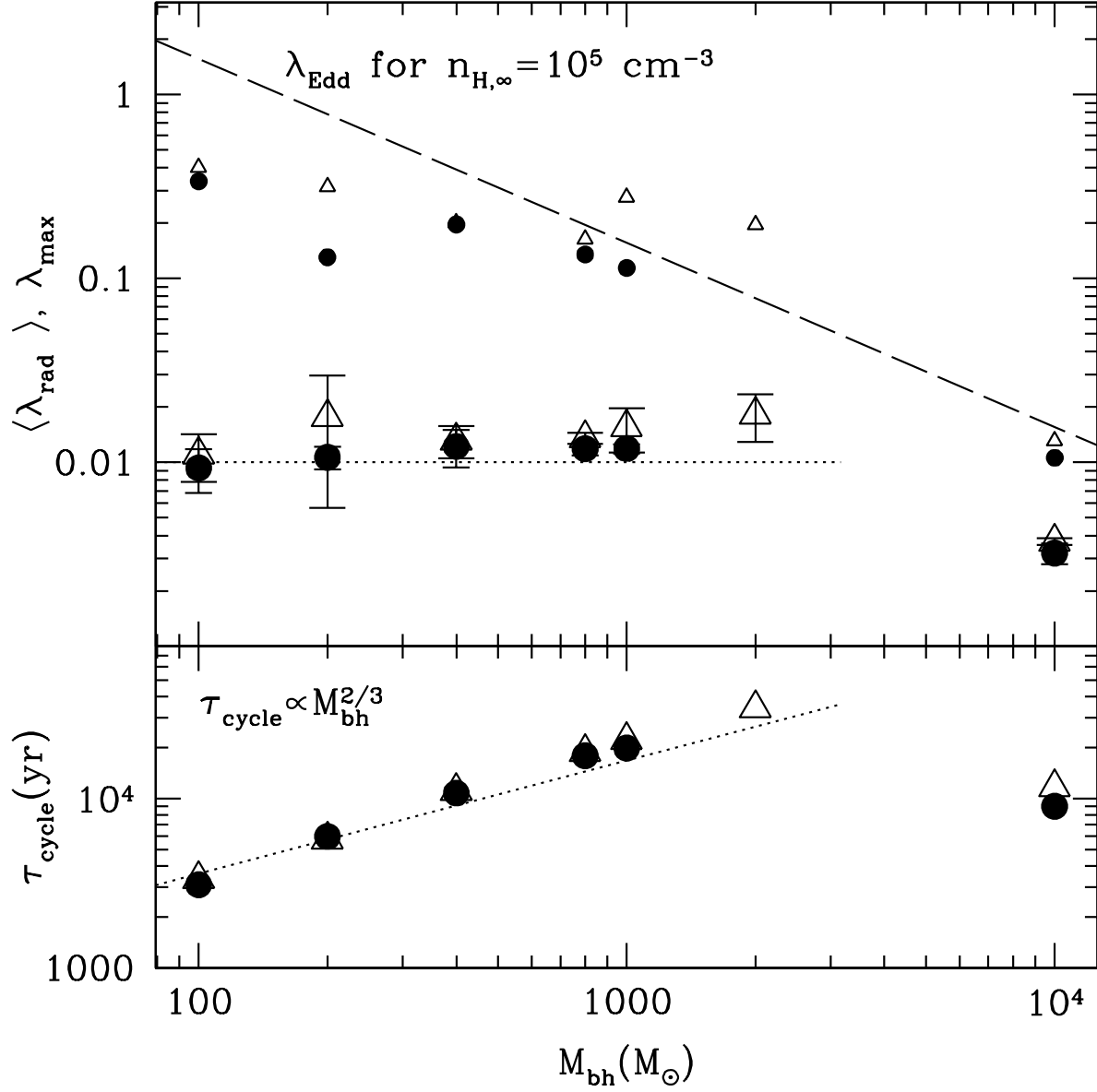
Fig. 3.— Same as Figure 1, but showing $\langle\lambda_{\rm rad}\rangle$, $\lambda_{\rm rad,max}$, and $\tau_{\rm cycle}$ as a function of $M_{\rm bh}$ with $\eta = 0.1$, $n_{\rm H,\infty} = 10^5$ cm^{-3}, and $T_\infty = 10^4$ K. A similar pattern which we observe as a function of density is also seen as a function of $M_{\rm bh}$. With increasing $M_{\rm bh}$, the transition from $\langle\lambda_{\rm rad}\rangle \sim 1\%$ to the Eddington-limited regime and the transition of $\tau_{\rm cycle}$ from mode-I to mode-II happen at $M_{\rm bh} \sim 4 \times 10^3\ M_\odot$.
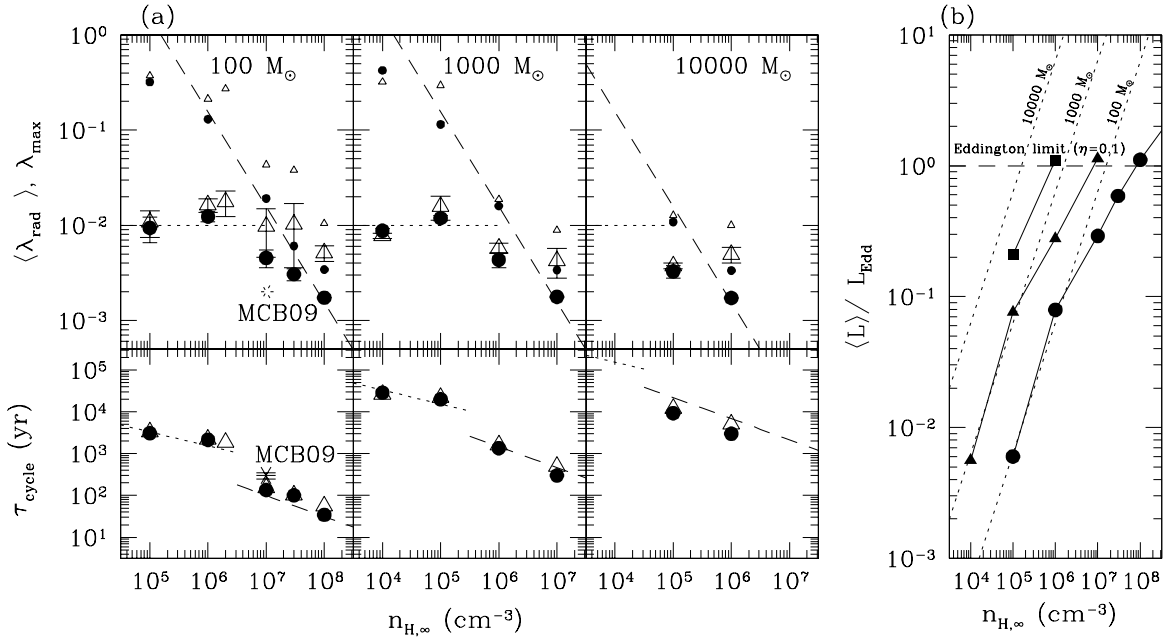
Fig. 4.— Left: same as Figure 2, but showing $\langle \lambda_{\mathrm{rad}} \rangle$, $\lambda_{\mathrm{rad,max}}$, and τ_{cycle} as a function of gas density for $M_{\mathrm{bh}} = 10^2 \ M_\odot$ (left panel), $10^3 \ M_\odot$ (middle panel), and $10^4 \ M_\odot$ (right panel). Long dashed lines in each panel show the Eddington accretion rate for $\eta = 0.1$ and the given BH mass. With increasing gas density, the accretion rate eventually becomes Eddington limited, but the transition to the Eddington-limited regime occurs at densities $n_{\mathrm{H},\infty}^{\mathrm{Edd}} \sim 4 \times 10^6 \ \mathrm{cm}^3 M_{\mathrm{bh}}^{-1}$ decreasing linearly with increasing BH mass. Right: accretion luminosities normalized by Eddington luminosities for the same simulations in the left figure. Symbols (circles: $10^2 \ M_\odot$, triangles: $10^3 \ M_\odot$, squares: $10^4 \ M_\odot$) show the simulations including radiation pressures for each BH mass. With increasing gas density, the accretion rate becomes regulated primarily by Compton radiation pressure.
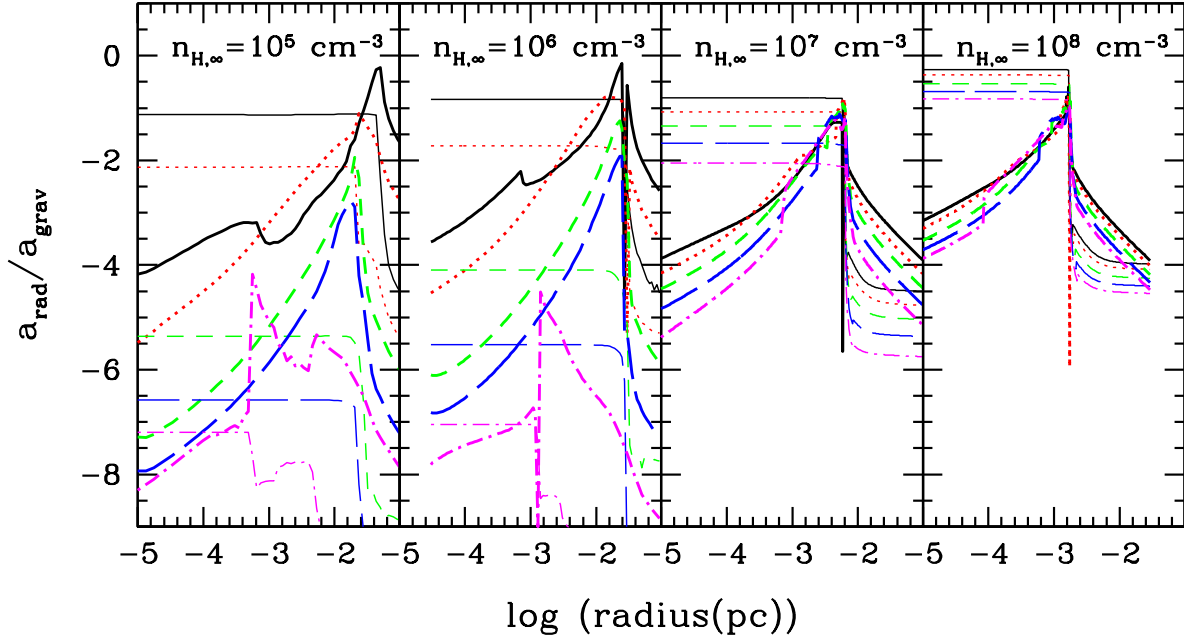
Fig. 5.— Radial profiles of the gas acceleration due to radiation pressures on H I and e^- normalized to the gravitational acceleration of simulations for $n_{\mathrm{H},\infty} = 10^5, 10^6, 10^7,$ and 10^8 cm^{-3} with BH mass $M_{\mathrm{bh}} = 100\ M_\odot$, $\eta = 0.1$, and $T_\infty = 10^4$ K. Thick lines refer to radiation pressure on H I, while thin lines show Compton scattering radiation pressure. Different line types show the profiles at different time during the oscillation cycle (e.g., solid lines at the accretion bursts and dot-dashed just before the bursts). Radiation pressure on H I peaks just inside the Strömgren sphere with weak dependence on density. While Compton radiation pressure inside the Strömgren sphere increases on average as a function of density. At $n_{\mathrm{H},\infty} = 10^7$ cm^{-3} the peak values of H I radiation pressure and Compton radiation pressure become comparable and about 10% of gravity. However, at higher densities ($\geq 10^8$ cm^{-3}) radiation pressure on electrons becomes dominant everywhere inside the Strömgren sphere.
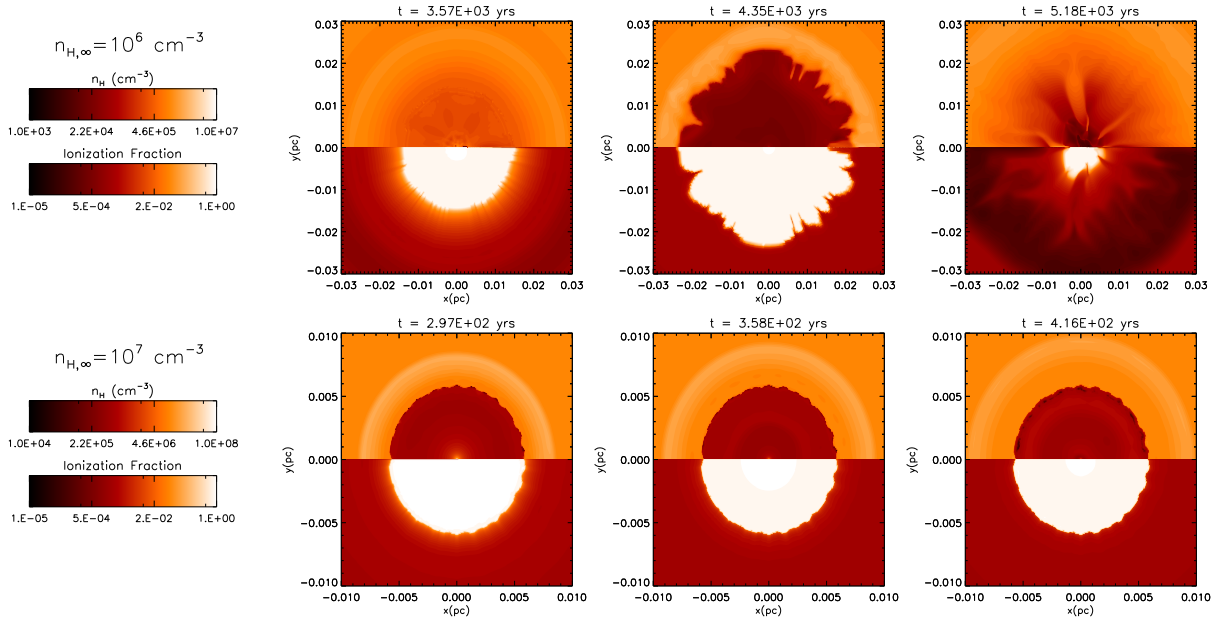
Fig. 6.— Illustration of the two different modes of oscillations found at different ambient densities. The panels show the time evolution of gas density and ionization fraction in 2D simulation for a BH of mass $M_{\rm bh} = 100\ M_\odot$, gas density $n_{\rm H,\infty} = 10^6$ cm^{-3} (top panels), and $n_{\rm H,\infty} = 10^7$ cm^{-3} (bottom panels). In each panel, top halves show the density and the bottom halves show the ionization fraction, $x_{\rm H\ II} = n_{\rm H\ II}/n_{\rm H}$. When the density is $n_{\rm H,\infty} \leq n_{\rm H,\infty}^{\rm cr} \simeq 5 \times 10^6$ cm^3, the collapse of ionization front onto the BH leads to a burst of accretion luminosity (mode-I). For densities $n_{\rm H,\infty} > n_{\rm H,\infty}^{\rm cr}$ the size of Strömgren sphere does not change much with time (mode-II). Note the different oscillation modes of the accretion rate and luminosity are driven by the collapse of dense shell (mode-I) and by a density wave (mode-II).
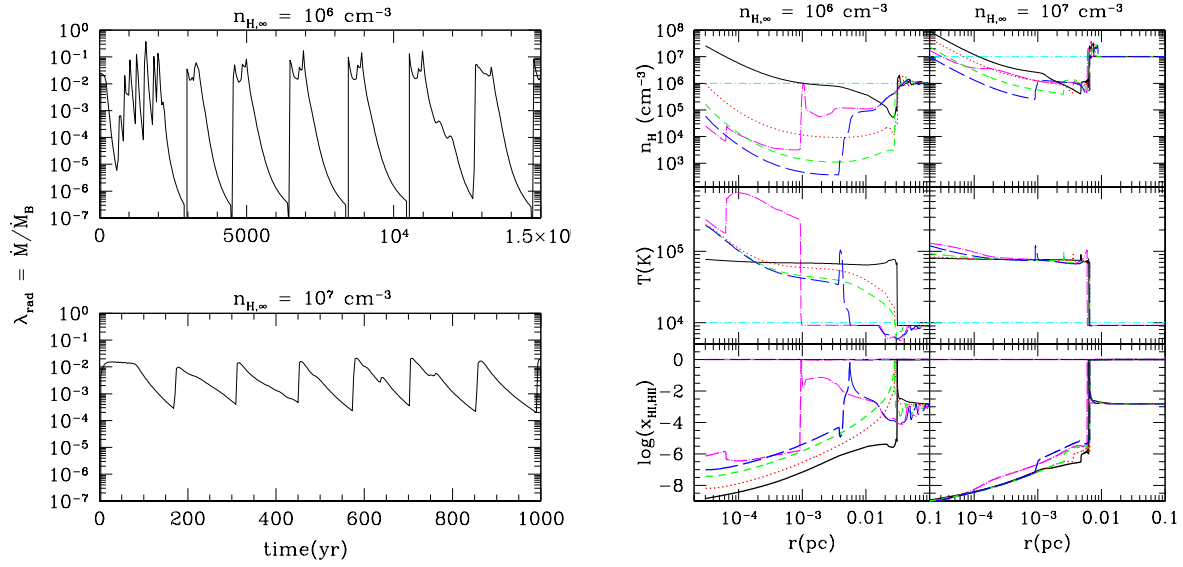
Fig. 7.— Left: accretion rates as a function of time for $n_{\mathrm{H},\infty} = 10^6$ cm^{-3} and $n_{\mathrm{H},\infty} = 10^7$ cm^{-3} assuming $\eta = 0.1$, $M_{\mathrm{bh}} = 100\ M_\odot$, and $T_\infty = 10^4$ K. Different modes of oscillations occur at different density regimes. Mode-I oscillation at $n_{\mathrm{H},\infty} = 10^6$ cm^{-3} shows about 5 orders of magnitude range between peak and the minimum accretion rate, while mode-II oscillation at $n_{\mathrm{H},\infty} = 10^7$ cm^{-3} shows only 2 orders of magnitude range. Right: evolution of radial profiles for density (top panel), temperature (middle panel), and neutral/ionization fractions (bottom panel) of the same simulations in the left figure. Note the change of physical properties inside Strömgren sphere during a period of mode-I oscillation ($n_{\mathrm{H},\infty} = 10^6$ cm^{-3}), while mild changes are observed for mode-II oscillation ($n_{\mathrm{H},\infty} = 10^7$ cm^{-3}).
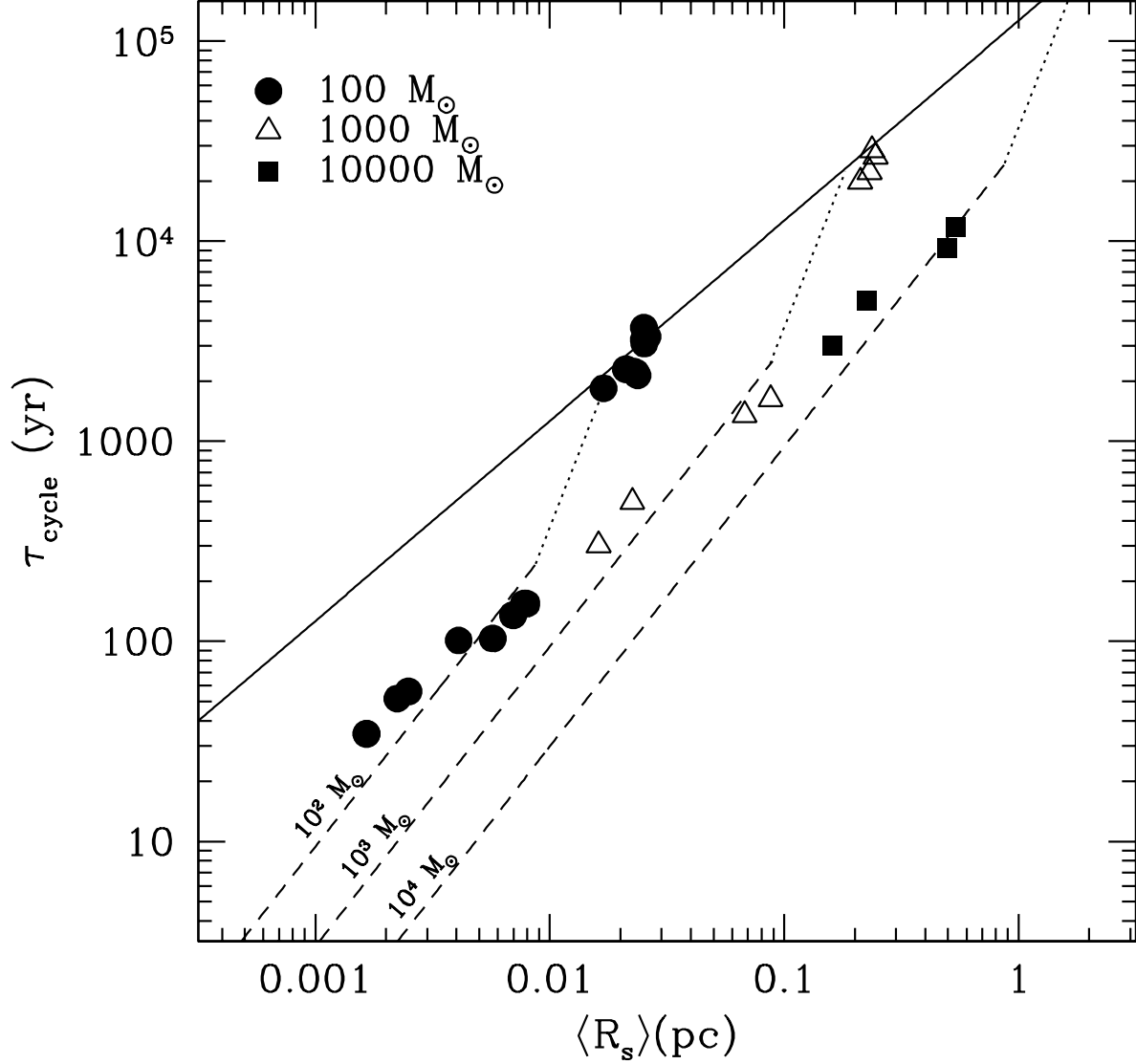
Fig. 8.— Relationship between the period of the accretion bursts, τ_{cycle}, and the time-averaged size of Strömgren radius $\langle R_s \rangle$. τ_{cycle} shows a linear relation with $\langle R_s \rangle$ when the gas depletion inside the Strömgren sphere is dominated by a pressure gradient inside the H II region that push the gas toward the I-front. Instead, $\tau_{\text{cycle}} \propto \langle R_s \rangle^3$ (dotted lines for each M_{bh}) when the gas depletion is dominated by accretion onto the BH. With increasing density of the ambient gas, for each M_{bh}, the transition to mode-II oscillation and the transition to Eddington-limited regime happen at similar densities $n_{\text{H},\infty} = n_{\text{H},\infty}^{\text{cr}} \sim n_{\text{H},\infty}^{\text{Edd}}$. In the Eddington-limited regime τ_{cycle} becomes proportional to $\langle R_s \rangle^{3/2}$ for each BH mass (dashed lines).
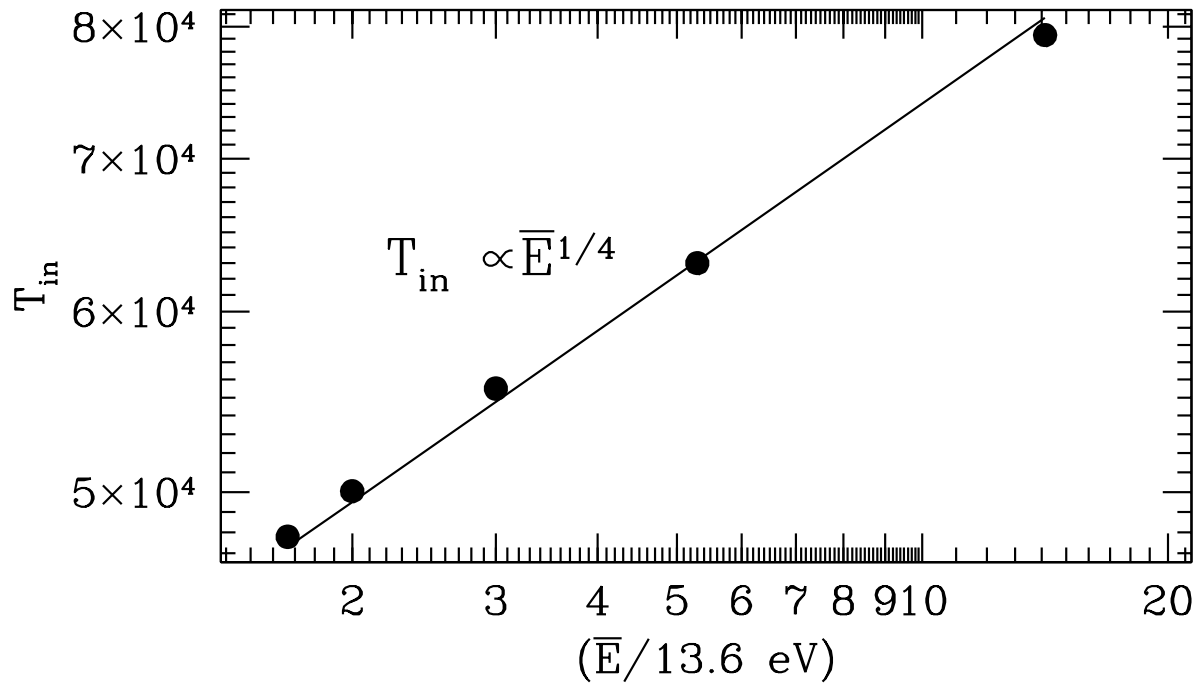
Fig. 9.— Temperature T_{in} at the effective inner Bondi radius, located inside the H II region produced by the accreting BH, as a function of the mean energy of ionizing photons $\bar{E}$ of the spectrum of radiation emitted near the BH by the accretion disk. We have assumed a gas of nearly zero-metallicity and a power-law spectrum $F_\nu \propto \nu^{-\alpha}$.
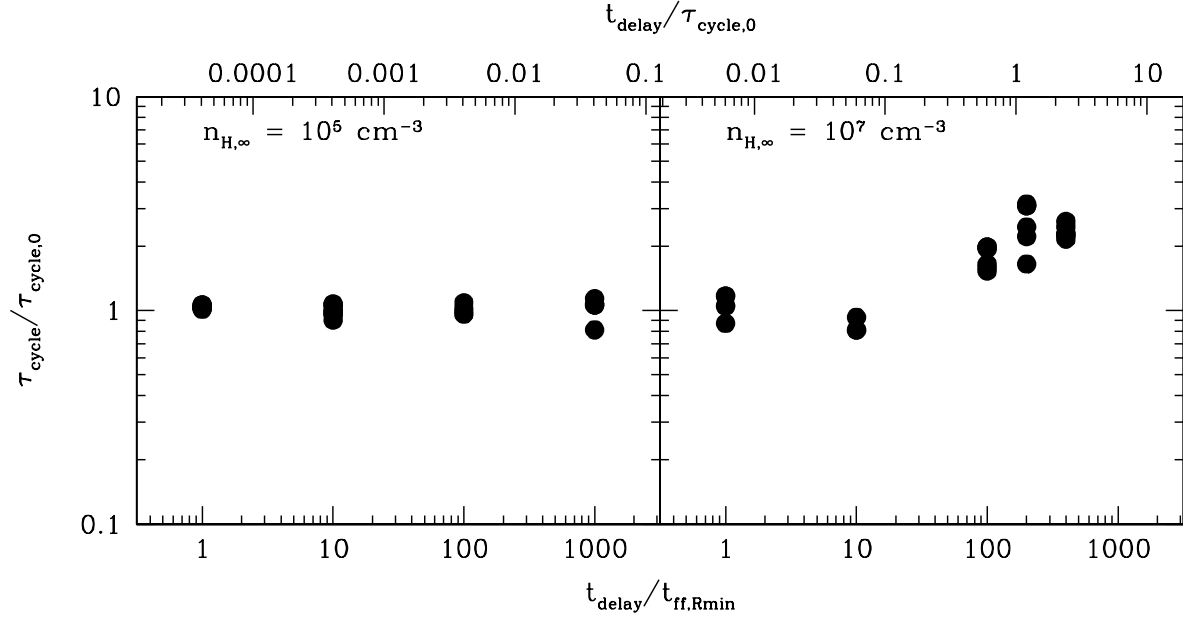
Fig. 10.— Dependence of the period between bursts τ_{cycle} on the time delay between the accretion rate at R_{min} and the BH output luminosity. The time delay is produced by the presence of the accretion disk that is unresolved in our simulations. The two panels show τ_{cycle} in units of $\tau_{\mathrm{cycle},0} \equiv \tau_{\mathrm{cycle}}(t_{\mathrm{delay}} = 0)$ as a function of t_{delay} for $n_{\mathrm{H},\infty} = 10^5 \ \mathrm{cm}^{-3}$ (left panel) and $10^7 \ \mathrm{cm}^{-3}$ (right panel). The bottom axis shows t_{delay} in units of the free-fall time at R_{min} and the top axis in units of $\tau_{\mathrm{cycle},0}$. The introduction of a time delay does not change τ_{cycle} when the gas density is $n_{\mathrm{H},\infty} = 10^5 \ \mathrm{cm}^{-3}$, while τ_{cycle} increases by approximately the amount of time delay introduced for $n_{\mathrm{H},\infty} = 10^7 \ \mathrm{cm}^{-3}$. In this density regime, the largest time delays introduced are comparable to the oscillation period $\tau_{\mathrm{cycle},0}$. In both cases, the oscillatory behavior of the accretion luminosity does not disappear.